

State to state photodissociation of H₂O in the first absorption band

D. Häusler, P. Andresen, and R. Schinke

Citation: *The Journal of Chemical Physics* **87**, 3949 (1987); doi: 10.1063/1.452949

View online: <http://dx.doi.org/10.1063/1.452949>

View Table of Contents: <http://scitation.aip.org/content/aip/journal/jcp/87/7?ver=pdfcov>

Published by the [AIP Publishing](#)

Articles you may be interested in

[H₂O photodissociation in the first absorption band: Entangled trajectory molecular dynamics method](#)

J. Chem. Phys. **138**, 024103 (2013); 10.1063/1.4774023

[New aspects of the photodissociation of water in the first absorption band: How strong is excitation of the first triplet state?](#)

J. Chem. Phys. **109**, 6641 (1998); 10.1063/1.477315

[Nonadiabatic effects in the photodissociation of H₂S in the first absorption band: An ab initio study](#)

J. Chem. Phys. **98**, 5508 (1993); 10.1063/1.465063

[Photodissociation dynamics and emission spectroscopy of H₂S in its first absorption band: A time dependent quantum mechanical study](#)

J. Chem. Phys. **93**, 6520 (1990); 10.1063/1.459678

[Photodissociation of vibrationally excited water in the first absorption band](#)

J. Chem. Phys. **91**, 7630 (1989); 10.1063/1.457233



State to state photodissociation of H₂O in the first absorption band

D. Häusler, P. Andresen, and R. Schinke

Max-Planck-Institut für Strömungsforschung, Bunsenstrasse 10, D-3400 Göttingen, Federal Republic of Germany

(Received 7 April 1987; accepted 17 June 1987)

The photodissociation of H₂O in the first absorption band is studied from single rotational states of vibrationally excited water. A tunable IR laser is used to prepare single rotational states in the asymmetric stretch mode. The subsequent photodissociation at 193 nm favors product formation from these single prepared states. The formation of the OH product in different rotational, Λ -doublet, and spin states is analyzed for a series of initial rotational states of H₂O. This is the first direct photodissociation studied on a state to state level. The product state distributions depend sensitively upon the prepared state in the parent molecule H₂O and exhibit pronounced quantum structure. The experimental results are understood almost quantitatively in terms of theory. The photodissociation of water turns out to be a limiting case of a dissociation which is governed by transfer of parent motion to products. The experiment leads to a highly improved understanding for the selective population of Λ -doublet states.

I. INTRODUCTION

Although photodissociation has been studied for a long time, state to state studies on the dynamics of photodissociation processes became possible only recently. These studies require the preparation of parent molecules in single quantum states and a state selective detection of products, which can be achieved with modern laser technology.

For the case of predissociation, preparation of initial quantum states is possible by the excitation to well defined rotational states in the upper electronic state.¹ Here we investigate a direct dissociation, where only one bound and one repulsive potential energy surface are involved. Preparation of the parent molecule can be done by several methods. In some cases jet cooling² yields a reasonable, but often incomplete state preparation. More powerful is the preparation of parent molecules via methods like IR excitation,³ CARS,⁴ and stimulated emission pumping.⁵ With these methods it is possible to achieve > 10% population in vibrationally excited states. In the present case IR excitation is used to prepare single rotational and vibrational states of H₂O in the electronic ground state.

For the analysis of the product state distributions, both laser induced fluorescence (LIF)⁶ and resonance enhanced multiphoton ionization (REMPI)⁷ are sensitive and state selective detection methods. With pulsed dissociation and pulsed detection a time resolution in the 10 ns range is easily obtained, which allows collision free analysis of products at higher pressures with good signal to noise.

Photodissociation processes consist essentially of two steps. The first step is the absorption of a photon leading to an excited state. The second step is the subsequent dissociation of this complex to the products. Equation (1) shows the case for the triatomic molecule ABC:



Here i is the initial quantum state from which the dissociation starts, $h\nu$ is the photon energy, ABC* the excited molecule, and f is one of the quantum states in which the product AB is formed.

The left-hand side of Eq. (1) shows that there are only two important parameters which govern the photodissociation process and determine both products and their state distributions: the photon energy $h\nu$ and the initial quantum state i .

The importance of the photon energy for the fragmentation has been recognized for a long time⁸: Depending on its energy content, the excited complex may fragment in many different ways. Either chemically different products (for example, AC + B) can be formed, or the partitioning of available energy over vibrational, rotational, or electronic states may be different at different photon energies.

Much less is known about the importance of the initial quantum state i of the parent molecule for the fragmentation process, essentially because there are considerable experimental difficulties in the preparation of single quantum states. In several experiments the crucial role of the rotational states of the parent molecule has been elucidated by comparison of bulk (300 K) with nozzle experiments.⁹⁻¹¹ Thus far a complete preparation of initial quantum states has been achieved only in the case of the first absorption band of H₂O.^{12,13}

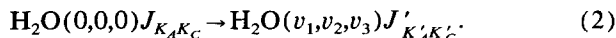
In this paper we use a new technique that allows us to study the photodissociation of molecules in single, preselected rotational states. Infrared excitation is used to prepare a single rotational quantum level in vibrationally excited water. This is followed by subsequent dissociation from this state. Although the present experiment is done for the first absorption band of H₂O, the general idea can be applied in other systems as well.

A qualitative dependence of the OH product state distribution on the rotational temperature of H₂O has been observed in two recent experiments.⁹ Whereas the photodissociation of jet-cooled H₂O gave rotationally cold OH and a high inversion among the Λ doublets, the photodissociation of H₂O at room temperature resulted in warmer OH and equal population among the Λ doublets. This indicates that the fragmentation does depend on the H₂O quantum state. Since the vibrational spacing of H₂O is fairly large, no excited vibrational levels are populated in either of the two ex-

periments. The *only differences* in the two experiments are the *rotational temperatures*.

In this experiment we study this dependence. Different rotational states of H₂O are prepared and the OH state distribution is detected. All other experimental parameters, such as the vibrational state and the photon energy are kept fixed. As will be shown, the OH state distributions are very sensitive to the rotational state of water.

The experimental procedure is as follows. In the first step H₂O is vibrationally excited to a well defined rotational state with a tunable IR laser. With quantum numbers (ν_1, ν_2, ν_3) for vibration and (J, K_A, K_C) for rotation this implies an IR transition¹⁴:



At room temperature no H₂O molecules are vibrationally excited, therefore only one rotational state, i.e., $J'_{K'_A K'_C}$, is populated in the vibrationally excited state.

The prepared H₂O is then photodissociated using 193 nm ArF excimer light. This wavelength is chosen such that the *absorption is large from vibrationally excited species, and small from the vibrational ground state*,¹⁵ so that products are obtained from the single quantum state prepared by IR excitation. A third OH probe laser is used to determine the product state distribution by LIF.

The photodissociation of H₂O in the first absorption band is a particularly interesting system to study for several reasons. The experimentally found inversion among the Λ doublets in jet cooled dissociation of H₂O is responsible for OH maser action in interstellar space.¹⁶ A prediction of the temperature dependence of the inversion is important for astrophysical applications. This can be done by simulating the photodissociation of H₂O at any initial temperature out of the state to state data.

The photodissociation of H₂O in the first absorption band is a model system for simple fragmentation processes. Only one bound and one repulsive excited state is involved and the latter is well isolated from all other states.¹⁷ Because the potential surface is strongly repulsive, the fragmentation is fast and direct, leading exclusively to the ground state products OH and H. The system is small enough to be treated by exact quantum mechanical methods, for the determination of *ab initio* potential surfaces¹⁷ and for the treatment of the dynamics on the surface.^{18,19}

The dissociation process can be divided into two steps. The first step is the photon absorption, described by a Franck–Condon transition from the H₂O ground state to the excited potential surface.^{20,21} The second step is the actual fragmentation on the repulsive potential surface. This is treated theoretically as a scattering process, which couples all degrees of freedom of the OH + H system. A new Franck–Condon model,²² which includes the electronic structure of the problem, reproduces the experimental rotational and fine structure distributions excellently, and allows a deeper understanding of the origin for the selective population of electronic fine structure states.

This is the first time that a photodissociation process is proved to behave according to the Franck–Condon approximation. Here clearly the second step treating the inelastic

half-collision during the fragmentation is negligible. For the rotational degree of freedom the torque acting on OH and also the coupling between the OH fine structure states are small during the fragmentation. A close look at the *ab initio* potential surface explains this behavior nicely, as will be shown later.

Because the dissociation of H₂O can be treated in the Franck–Condon limit, the details of light absorption to a repulsive state and the influence on the fragment state distribution can be learned. Within the Franck–Condon approximation we perform model calculations and try to gain an idea of how similar molecules dissociate.¹¹

II. EXPERIMENTAL

A. Apparatus

Figure 1 shows the experimental setup, essentially a simple flow system operated at room temperature. It is a small stainless steel tank with 100 mm inner diameter, evacuated by a roughing pump. Water is admitted into the tank through a needle valve and the H₂O pressure is measured with a baratron gauge and is typically 0.04 Torr. CaF₂ windows on the tank are used to transmit both infrared and UV light.

The use of a flow system at room temperature has the advantage that many different rotational states can be prepared in vibrationally excited H₂O. In a supersonic beam only a few low rotational states are available.

The three laser beams are collinear with the IR laser, antipropagating to both the ArF excimer and the OH probe laser. A central timing mechanism triggers all lasers jitter-free. Typically the lasers are fired with 50 ns delays between each other, in the sequence IR, ArF, and OH probe laser.

The tunable infrared laser consists of an excimer pumped dye laser (EMG 200, FL 2002E) which, when operated with an étalon, gives a pulse energy of ≈ 50 mJ in a linewidth of 0.04 cm^{-1} . The dye output is focused in a Raman shifter, filled with 18 bar H₂. To improve the Raman efficiency, a wave guide is mounted in the Raman cell.²³ The third Stokes line is separated from other Stokes and the fundamental line by a coated germanium plate. Operating the

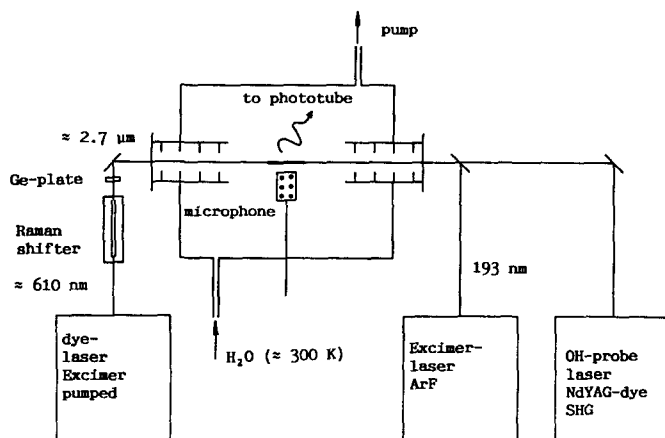


FIG. 1. Experimental setup for the photodissociation of single quantum states of H₂O.

dye laser around 610 nm yields ≈ 0.5 mJ/pulse tunable infrared at $2.7 \mu\text{m}$ with the same linewidth of 0.04 cm^{-1} . The beam path of the IR laser is flushed with dry N₂ to prevent absorption of water in air.

The ArF excimer laser (EMG 200 Lambda Physik) delivers ≈ 400 mJ/pulse. The OH product state distribution is probed by a tunable UV laser in the same way as before.⁹ Fluorescence is collected at a right angle to the laser beams using imaging optics. The signal of the phototube is sent to a boxcar and subsequently recorded on a strip chart recorder.

B. IR excitation

Water has a strong absorption band at $2.7 \mu\text{m}$ where the symmetric (100) and asymmetric stretches (001) as well as the first overtone of the symmetric bend (020) are excited. The absorption cross sections for some strong lines of the different vibrational states are given in Table I.^{24,25}

The molecular transitions are Doppler broadened with a linewidth of 0.009 cm^{-1} . The estimated excitation efficiencies when the laser is slightly focused to a spot of 0.1 cm^2 are also given in Table I. Note that the excitation of the asymmetric stretch is an order of magnitude more efficient than for the other vibrational modes.

The IR excitation is monitored using the photoacoustic technique.²⁶ A microphone is mounted in a separate cell containing ≈ 5 Torr H₂O. The IR laser passes through this cell close to the microphone. Whenever the laser frequency matches an IR transition in H₂O, water molecules are vibrationally excited along the beam path. Relaxation processes cause a sound wave to be emitted which is recorded by the microphone. The photoacoustic technique is used to mark the IR laser frequencies at which water is vibrationally excited. With the well known IR spectra of H₂O^{24,25} it is easy to identify the lines.

We also measured the excitation ratio of 7% and the absorption cross section $\sigma_{\bar{\nu}} d\bar{\nu} = 4.1 \times 10^{-20} \text{ cm}$ for one vibrational transition $\nu = 000$, $J_{K_A K_C} = 2_{02} \rightarrow \nu = 001$, $J_{K_A K_C} = 1_{01}$. This is close to the literature value of $6.4 \times 10^{-20} \text{ cm}$,²⁵ and gives considerable faith in the excitation ratios listed in Table I.

C. Absorption probabilities for 193 nm

As mentioned above, the idea of the experiment relies on a large difference between the absorption from the vibrational ground state and the vibrationally excited states. The qualitative explanation for the large difference in the absorption is given in Fig. 2. This correlation diagram shows schematically the two potential surfaces A' and A'' , as well as the

TABLE I. Absorption cross sections for strong lines in the IR spectrum in the excitation of different vibrational modes of H₂O at $2.7 \mu\text{m}$ (Refs. 24 and 25).

Vibrational transition	Rotational transition	Wavelength (cm ⁻¹)	$\int \sigma_{\bar{\nu}} d\bar{\nu}$ 10 ⁻²⁰ (cm)	Excitation efficiency
(000) → (001)	3 ₀₃ → 4 ₀₄	3837.87	23.9	27.5%
(000) → (020)	1 ₁₀ → 1 ₀₁	3133.07	0.146	0.17%
(000) → (100)	3 ₂₁ → 4 ₂₂	3835.57	1.85	2.11%

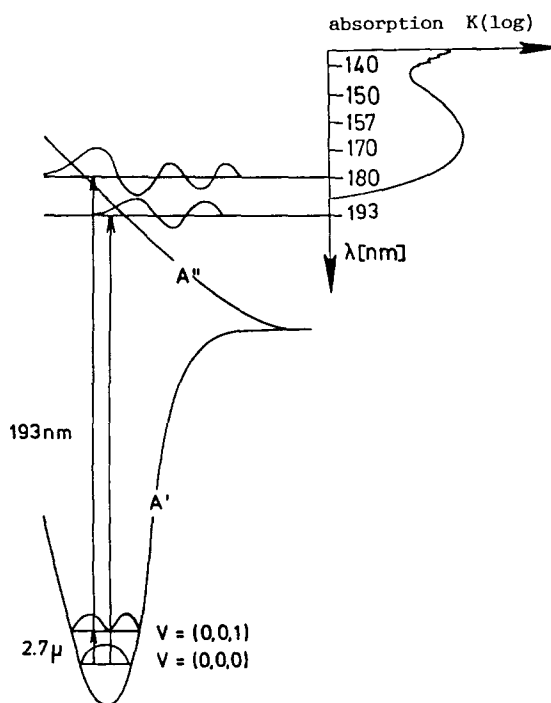


FIG. 2. Idea of the experiment. For the electronic ground state of H₂O the nuclear wave functions are shown for the vibrational ground and excited state. The $2.7 \mu\text{m}$ correspond to the IR excitation in the experiment. From the vibrational ground state a lower energy is reached after excitation with the 193 nm light than from the vibrationally excited state. The scattering wave function is shown for both cases. At the right side the absorption of H₂O in the first band in the VUV is shown.

absorption cross section of room temperature H₂O¹⁵. For the electronic ground state A' , the nuclear wave functions are shown for the vibrational ground and excited state. The two nuclear wave functions for the electronically excited state A'' are also shown for the transition from the vibrational ground (lower) and the vibrationally excited (upper) state.

As can be seen in the figure, water starts to absorb around 185 nm. The classical turning point of the corresponding scattering wave function at the wavelength used in this experiment, 193 nm, is at such large internuclear distances, that the overlap of the ground state and scattering wave functions is poor. The classical turning point is shifted to smaller internuclear distances and the overlap of the two wave functions is much better, with additional vibrational energy from the IR excitation. This increases the energy of the excited complex to a wavelength of approximately 180 nm when H₂O is excited from the ground vibrational state. This qualitatively explains the highly enhanced absorption from vibrationally excited H₂O at 193 nm. Quantum mechanical *ab initio* calculations predict an increase by a factor of about 500 for the absorption for H₂O excited in the asymmetric stretch mode compared to the vibrational ground state.²⁷

In the experiment there will be absorption both from vibrational ground and vibrationally excited states of H₂O. Because the population in vibrationally excited states of H₂O is negligible at room temperature, the only molecules that are vibrationally excited are those prepared by IR excitation. This is, however, only a small fraction of all H₂O molecules.

The water molecules in the vibrational ground state give a dissociation signal too, which is here a noisy background signal. The noise of this signal is mainly due to the power fluctuations of the ArF laser, typically on the order of 10%. When the OH signal from a single vibrational excited state is larger than 10% of the background signal, the signal to noise ratio is about 1 and the detection can be done without great effort.

The two relative contributions to the OH signal can be estimated easily. At 300 K, 2% of the H₂O molecules are in a particular rotational state, at least for the states considered here. The excitation to the asymmetric stretch mode has an efficiency of $\approx 10\%$ (see Table I), which implies that 2×10^{-3} of the H₂O molecules are prepared in the vibrationally excited state. However, because the absorption from this vibrationally excited state is enhanced by a factor of ≈ 500 compared to the vibrational ground state, the signal from the prepared vibrationally excited state will be in the same order of magnitude as the signal from all other states in the vibrational ground state together. In good agreement with these qualitative arguments, we observe 2–3 times more signal from the vibrationally excited H₂O in the experiment.

For the symmetric stretch and the bending mode the excitation efficiency is much lower. Consequently, the ratio is much smaller and the discrimination between ground state photolysis and photolysis from the prepared states is much harder. This is the reason for the choice of the asymmetric stretch excitation in the present experiment.

D. Data collection

The experimental procedure is as follows: In the first step we prepare the vibrationally excited state by tuning the IR laser to an IR transition. The photoacoustic method is used to identify the transitions and to optimize the laser on the IR line.

In Fig. 3 a photoacoustic IR scan [3(b)] is compared with an IR spectrum of H₂O taken from Refs. 24 and 25 [3(a)]. The identification of lines is simple and the corresponding rotational quantum numbers are labeled above the lines. The upper label is for the vibrationally excited, here the asymmetric stretch vibration, and the lower label for the vibrational ground state.

The lowest curve [3(c)] shows the OH photodissociation product fluorescence, as observed on the R₁ line, as a function of the frequency of the IR vibrational pumping laser. The OH probe laser is fixed on the R₁ transition, the IR laser is scanned over the same range as before, with the excimer laser firing in between. The positions of the lines in curve 3(c) clearly correspond to those seen in the IR spectra 3(a) and 3(b). The OH fluorescence is enhanced when a vibrationally excited state is prepared by the IR laser. The peaks are clearly due to photodissociation out of single rotational states of the asymmetric stretch vibration. The quantum numbers of the prepared OH states correspond to the upper labels in Fig. 3(b). Curve 3(c) demonstrates that photodissociation from single preselected states is possible.

Obviously the peak heights are different for these three spectra. The photoacoustic spectra are used here only for frequency calibration and their intensity is not expected to

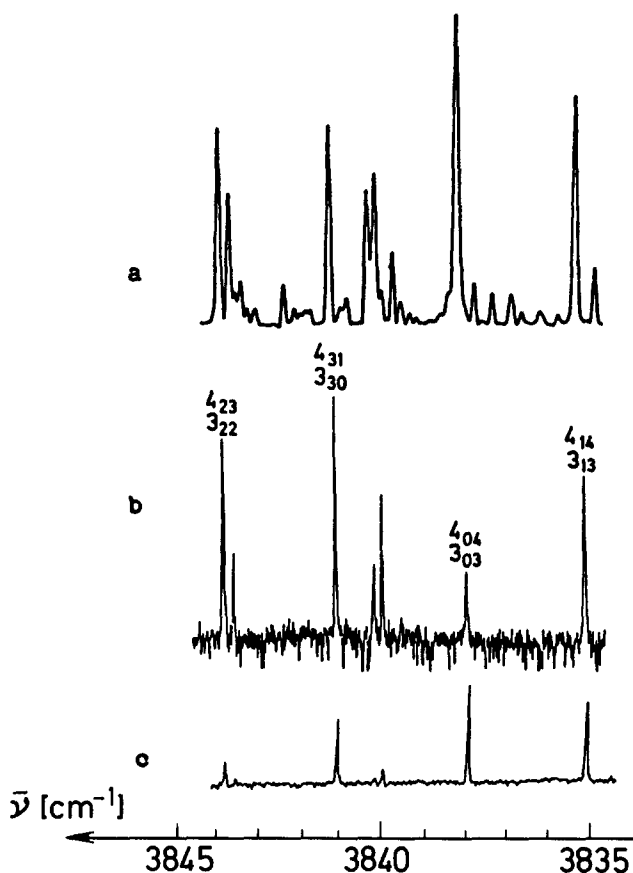


FIG. 3. IR scans between 3834.5 and 3843.8 cm⁻¹. The upper trace (a) shows an IR spectrum of H₂O from the literature (Ref. 25). The trace in the middle (b) shows a photoacoustic scan with the quantum numbers for the IR transitions. The lower (upper) quantum numbers are for the vibrational ground (excited) state, respectively. The lowest trace (c) shows the OH fluorescence intensity on the R₁(1) line for all the three lasers operating. The IR laser is scanned.

reproduce the population of quantum states. The third spectrum is different because the formation of OH in a particular state (here the ${}^2\Pi_{3/2}$, $N=1, \Pi^+$ state), depends sensitively on the prepared state in H₂O (see below).

In general, the rest of the results reported here were obtained by keeping the IR laser fixed and scanning the OH probe laser over the OH (${}^2\Pi \rightarrow {}^2\Sigma$) absorption band. Using the R₁, Q₁, and R₂ branches, the rotational distributions of the ${}^2\Pi_{3/2}^{+,-}$ and ${}^2\Pi_{1/2}^{+}$ fine structure components are measured.²⁸ At OH angular momentum quantum numbers $N=4$ and $N=1$ the ratios of the three fine structure levels relative to each other are determined and the rotational distributions are normalized to each other. The ${}^2\Pi_{1/2}^{-}$ fine structure levels could not be measured, because of too many line overlaps.

Collision-free conditions were ensured by keeping the H₂O pressure at 0.04 Torr and the delay times between the laser firings at ≤ 100 ns. Doubling of the delay time or pressure did not alter the OH state distributions.

III. EXPERIMENTAL RESULTS

A. Photodissociation of room temperature H₂O at 193 nm

A small background signal was observed even with the IR laser off. This was attributed to direct absorption of H₂O

leading to photodissociation at 193 nm. Although the signals were weak, they were large enough to determine the OH product state distributions, shown in Figs. 4–6.

Figure 4 shows in a Boltzmann plot the population of OH formed in different rotational states for the two Λ doublet components in the $^2\Pi_{3/2}$ multiplet state. The position of the curves relative to each other is determined by an experimental calibration procedure. The rotational distributions are first measured independently for both Λ doublet states. Then the position of the two distributions relative to each other is determined at $N = 4$, by measuring the population in Π^- and Π^+ at $N = 4$ several times immediately after each other.

For both Λ doublet components the result can be fit with a straight line in a Boltzmann plot, indicating a Boltzmann distribution. For the Π^- Λ doublet we find a rotational temperature of 457 K, somewhat higher than that of 379 K for the Π^+ Λ doublet. For the photodissociation at 157 nm the rotational temperatures were found to be higher (960 K) and the same for both Λ doublet components.⁹ This will be discussed further below.

Figure 5 shows, as a function of the OH quantum number j , the ratio of the population in the upper and lower Λ doublet states. Because the signals are rather weak, the error bars are large. No value could be given for $j = 3.5$, due to poor spectral resolution.

In agreement with corresponding data for the photodissociation of cold H₂O at 157 nm,⁹ more OH is formed in the upper Λ doublet state. However, as mentioned before, no Λ doublet preference could be found for room temperature H₂O at 157 nm. This may be due to quenching of the Λ doublet distributions, which was recently found to be extremely fast.²⁹

Figure 6 addresses the question of selective spin popula-

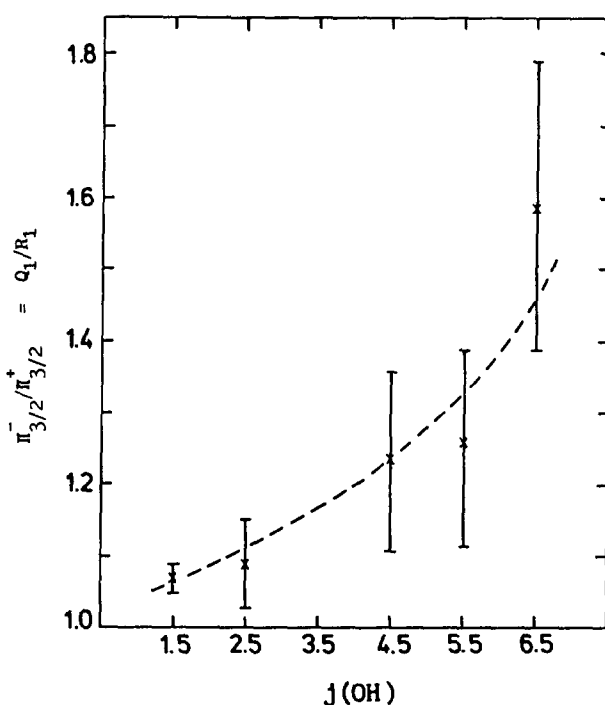


FIG. 5. Relative population in the two Λ doublet states in $^2\Pi_{3/2}$ for the photodissociation of room temperature H₂O at 193 nm. Shown is the ratio of Q line vs R line fluorescence intensity.

tion. The ratio of the population of the rotational states with quantum number N in $^2\Pi_{1/2}(N = j + 1/2)$ and $^2\Pi_{3/2}(N = j - 1/2)$ is plotted as a function of N . The degeneracy of the states is taken into account by the factor $N/(N + 1)$. A value of 1 corresponds to a statistical distribution. Although there may be a small preference for the $^2\Pi_{3/2}$ multiplet state, the error bars are too large for this to be certain. Thus no selective formation of OH in different spin states is found in this work, in agreement with earlier data.⁹

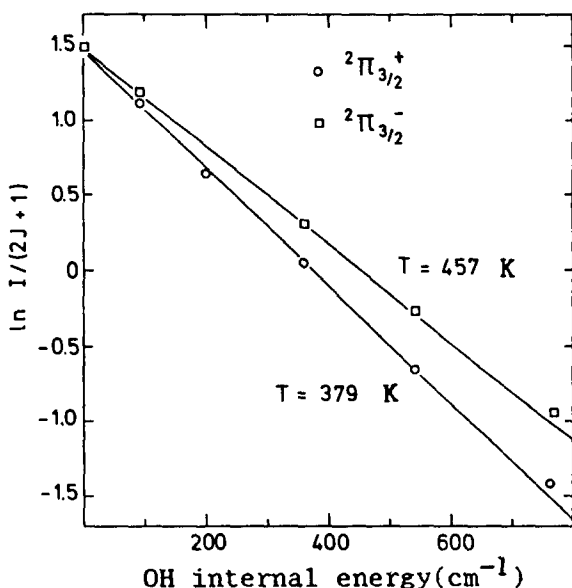


FIG. 4. H₂O photodissociation of room temperature H₂O at 193 nm. In a Boltzmann plot the rotational state distributions of the OH product are shown for the upper ($^2\Pi_{3/2}^+$) and lower ($^2\Pi_{3/2}^-$) Λ doublet states in the $\Omega = 3/2$ multiplet state. The temperatures are obtained from the slope of the lines.

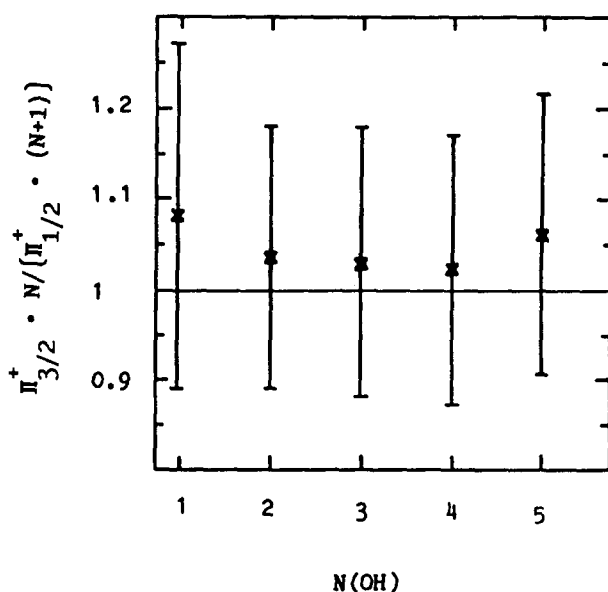


FIG. 6. Spin distribution in the OH product for the Π^+ Λ doublet. In the plot the quantum number N ($j = N + 0.5$ for $\Omega = 3/2$ and $j = N - 0.5$ for $\Omega = 1/2$) is used. The factor $N/(N + 1)$ takes the degeneracy of states into account, so that a value of 1 corresponds to a statistical distribution.

In contrast to the data at 157 nm, no population was found in $v = 1$. This is supported by recent calculations which predict no OH vibrational excitation for a wavelength larger than 175 nm.²⁷

B. Photodissociation of single quantum states of vibrationally excited water

The photodissociation of vibrationally excited H₂O (asymmetric stretch mode) is studied from several rotational states. We present data for the rotational ground state 0_{00} and for five states with total angular momentum $J = 4$ ($4_{04}, 4_{14}, 4_{23}, 4_{22}, 4_{31}$). The IR transitions used to prepare these states are given in Table II.

The experimental results in Figs. 7–9 show measured OH product state distributions. Figure 7(a) gives the rotational distributions for the dissociation of the rotational ground state 0_{00} . For the Λ doublet states probed by R lines, indicated by + sign, the population decreases with increasing OH rotational quantum number. For the other Λ doublet state, measured by Q lines, there is first an increase from $j = 1.5$ to $j = 2.5$ and a decrease later on.

With a few exceptions, in almost all experiments where a selective population of Λ doublet states has been found there was a consistent preference for one Λ doublet state, for example, Π^- . This is different here: An increase in the population of one Λ doublet coupled with a decrease in the population of the other Λ doublet implies that we are dealing with a j dependent change from inversion to anti-inversion.

The data for the other multiplet state ${}^2\Pi_{1/2}$ are also given in Fig. 7(a) for the Π^+ Λ doublet only. The similarity with the same Λ doublet population in ${}^2\Pi_{3/2}$ is obvious. If the appropriate statistical weights are taken into account (compare discussion for 193 nm) we obtain a spin distribution close to the statistical value of 1, as shown in Fig. 7(b).

Figure 8 shows experimental OH distributions for photodissociation from five different rotational states with the same total J ($J = 4$). The data are for the Π^+ Λ doublet in ${}^2\Pi_{3/2}$, i.e., the fluorescence is measured on R lines. The three quantum numbers represent the rotational state $J_{K_A K_C}$ of H₂O.

In contrast to almost all rotational distributions obtained from inelastic collisions, chemical reactions, or photodissociation processes, these distributions look very different. The almost erratic structure in these curves with different maxima and minima is real, because experimental errors are below 20%.

TABLE II. IR transitions used to prepare rotational states of water in the asymmetric stretch mode.

$v = (001)$ $J_{K_A K_C}$	$v = (000)$ $J_{K_A K_C}$	Wave number (cm ⁻¹)
0_{00}	1_{01}	3732.135 39
4_{04}	3_{03}	3837.870 25
4_{14}	3_{13}	3834.983 03
4_{23}	3_{22}	3843.751 40
4_{22}	4_{23}	3765.760 51
4_{31}	3_{30}	3841.045 16

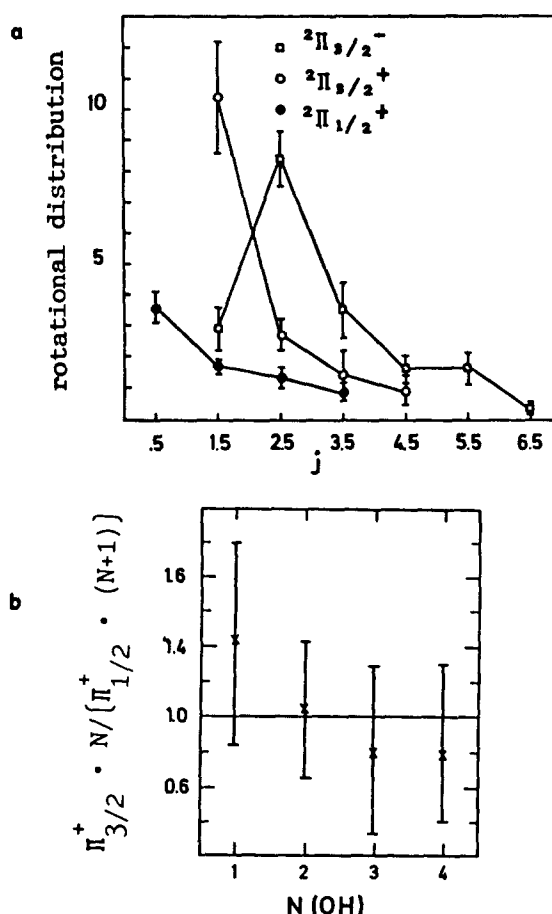


FIG. 7. OH product state distributions for the photodissociation of the 0_{00} state of H₂O in the asymmetric stretch mode. (a) shows the rotational distributions for the Π^- (open circles) and Π^+ (open squares) Λ doublet in ${}^2\Pi_{3/2}$ and for the Π^+ Λ doublet in ${}^2\Pi_{1/2}$ (full circles). (b) shows the corresponding spin distribution plotted in the same way as in Fig. 6.

Although all these states are rather close in energy and belong to the same total H₂O angular momentum $J = 4$, the OH product state distribution depend strongly upon the initially prepared state. It is certainly a surprise that every H₂O state yields completely different OH product state distributions.

For the three rotational states 4_{04} , 4_{14} , and 4_{31} we also measured the rotational distributions for other fine structure states. They are shown in Fig. 9. First we compare the population in the two Λ doublet states in ${}^2\Pi_{3/2}$. We find a similar oscillating behavior as going from $j = 1.5$ to $j = 2.5$ in the rotational ground state 0_{00} : the population in one Λ doublet is increasing, whereas the population in the other Λ doublet is decreasing. This effect is most pronounced at low j .

The population in the other multiplet state ${}^2\Pi_{1/2}$ is also given in Fig. 9. Obviously there is a close relation between the structure for the Λ doublet states probed by R lines (${}^2\Pi_{3/2}^+$ and ${}^2\Pi_{1/2}^+$). As in the case of the rotational ground state, the similarity is simply due to the statistical spin distribution: if appropriate statistical weights are taken into account, the distributions are the same within experimental error. This implies that even on a state to state basis the spin distribution is close to the statistical case.

The similarity between the OH state distributions for

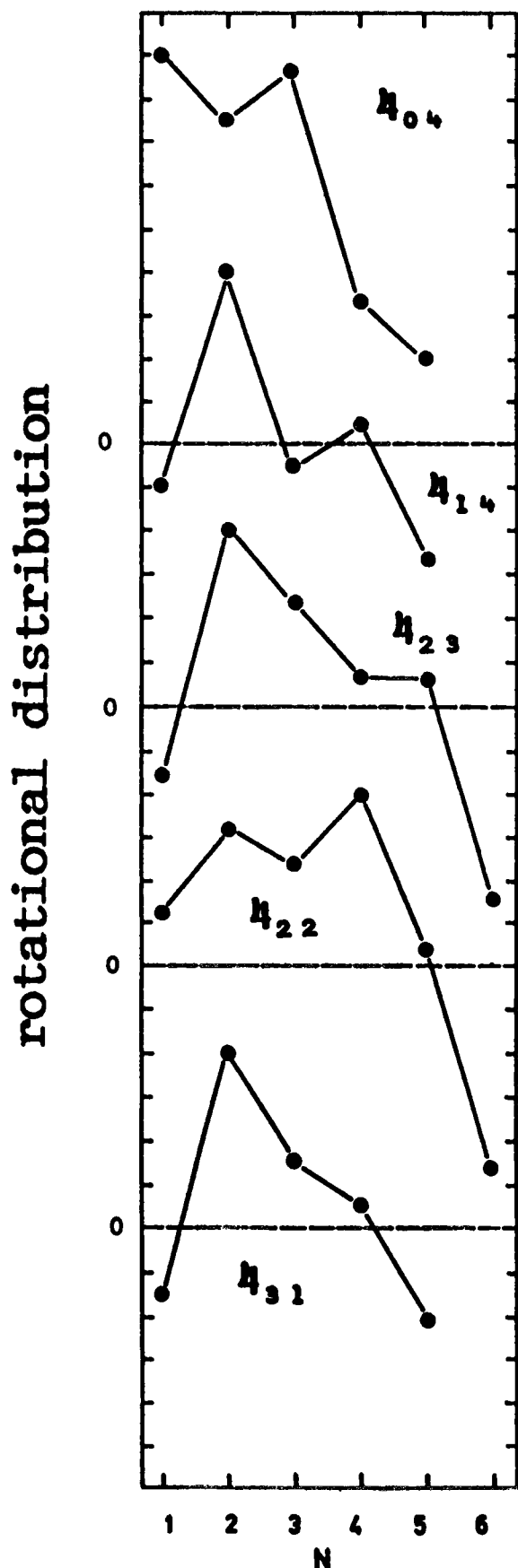


FIG. 8. OH product distributions for the Π^+ A doublet in $^2\Pi_{3/2}$ multiplet state (measured on R lines) for the H₂O photodissociation from several rotational states given in the figure.

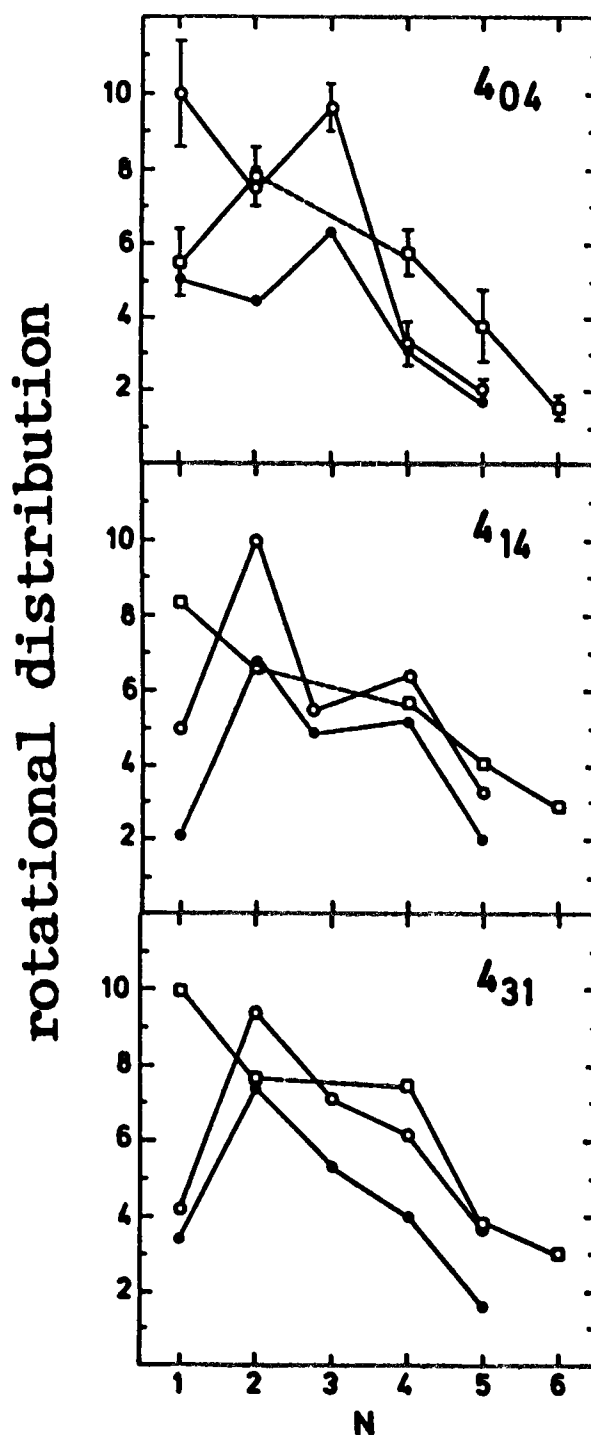


FIG. 9. Photodissociation of H₂O from the rotational states 4_{04} , 4_{14} , and 4_{31} for different electronic fine structure states of OH. Open circles are for the Π^+ A doublet of $^2\Pi_{3/2}$, open squares for the Π^- A doublet in the same spin state, and full circles for the Π^+ A doublet in $^2\Pi_{1/2}$.

the two multiplet states, which is simply a consequence of the statistical spin population, demonstrates also that the observed strong structure is real. Unfortunately no data are available for the $^2\Pi_{3/2}^-$ state, because there are too many line overlaps.

Although all experimental rotational distributions are strongly structured, with oscillating populations in the two A doublet components, Boltzmann distributions are already obtained if only the two A doublet components are averaged.

This is shown in Fig. 10. The quantum numbers for the initially prepared quantum states are given in the figure, together with the corresponding rotational temperature. The few data points that could be obtained are clearly lying on a straight line. This is a surprising result: The strong structure in the distributions vanishes completely simply by averaging over the Λ doublet components.

The rotational temperature calculated from the Boltzmann plot depends upon the initially prepared state. Whereas for states with $J(\text{H}_2\text{O}) = 4$ a value of about 370 to 460 K is obtained, the value of ≈ 190 K for the $J = 0$ state is clearly lower. Obviously part of the rotational energy contents in the parent molecule H₂O is transferred to the product OH.

IV. THEORY

As mentioned above, the photodissociation of water in the first absorption band can be treated by almost rigorous quantum mechanical methods. An accurate *ab initio* potential surface has been calculated, and the dimension of the system is still small enough so that exact quantum mechanical calculations are possible.^{18,19}

With $J_{K_A K_C}, \nu$ as quantum numbers for the H₂O bound state the distribution of the OH [$^2\Pi_{\Omega}^p(j)$] ($p = \pm 1$; $\Omega = 1/2, 3/2$) states is given by the Golden Rule:³⁰

$$P(J_{K_A K_C} \rightarrow \Omega, j, p) = |\langle \Phi^{\text{H}_2\text{O}}(J_{K_A K_C}, \nu) | \epsilon \cdot \mu | \Phi^{\text{OH}+\text{H}}(j, \Omega, p) \rangle|^2, \quad (3)$$

where $\Phi^{\text{H}_2\text{O}}(J_{K_A K_C}, \nu)$ is the wave function of the bound state and $\Phi^{\text{OH}+\text{H}}(j, \Omega, p)$ is the scattering wave function which asymptotically at large OH–H distances describes a OH molecule in the $^2\Pi_{\Omega}^p(j)$ state. In general these wave functions depend on nuclear (radial and angular) and electronic coordinates making the integral multidimensional and hard

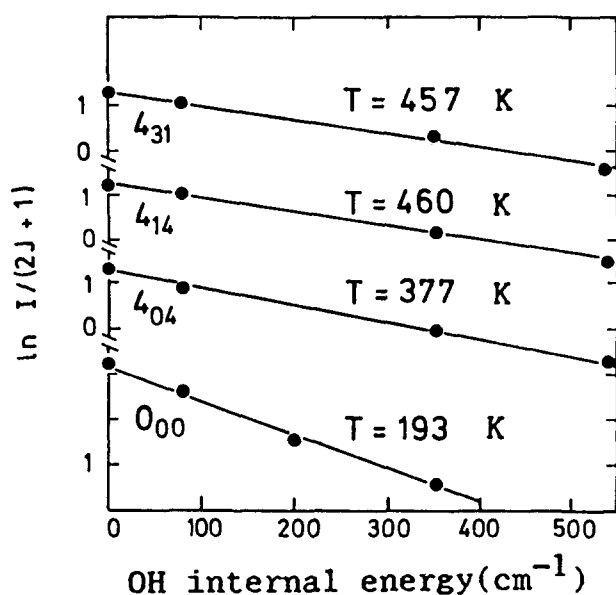


FIG. 10. A doublet averaged OH product state distributions. For each j the population in the two Λ doublets is averaged and plotted in a Boltzmann plot. The H₂O quantum states and the OH rotational temperature obtained for these states are given in the figure.

to solve. However, for the present case rotational and fine structure distributions can be calculated in the Franck–Condon limit for bound–continuum transitions. In this approximation Eq. (3) reduces to an integral over angular and electronic coordinates. In the following we show, how $\Phi^{\text{OH}+\text{H}}(j, \Omega, p)$ and $\Phi^{\text{H}_2\text{O}}(J_{K_A K_C}, \nu)$ can be separated into a radial and angular plus electronic part.

The bound state wave function decouples at least for small rotational and vibrational quantum numbers:

$$\Phi^{\text{H}_2\text{O}}(J_{K_A K_C}, \nu) = \Phi_{\text{rot}}(J_{K_A K_C}) \cdot \Phi_{\text{vib}}(\nu) \cdot \Phi_{\text{elec}}(A', A'') \quad (4)$$

in a product of vibrational, rotational, and electronic wave functions where A', A'' denote the symmetry of the H₂O potential. Φ_{rot} describes the rotation of the H₂O molecule in a space fixed frame and is a function of three angles. Φ_{vib} describes the vibrational motion and depends on both radial coordinates r, R from the (symmetric and asymmetric) stretch vibrations and on the H₂O bond angle γ from the bend motion:

$$\Phi_{\text{vib}}(\nu_1 \nu_2 \nu_3) = \Phi_{\text{bend}}(\nu_2; \gamma) \cdot \Phi_{\text{stretch}}(\nu_1, \nu_3; r, R). \quad (5)$$

If the bend vibration is not excited ($\nu_2 = 0$), $\Phi_{\text{bend}}(0; \gamma)$ is a Gaussian-like function peaking at the H₂O bond angle $\approx 104^\circ$, with a FWHM of about 25° describing the zero point motion.

The angular and electronic part of the bound H₂O wave function separates with Eqs. (4) and (5) into a radial and electronic-angular part:

$$\Phi^{\text{H}_2\text{O}}(J_{K_A K_C}, \nu) = \{ \Phi_{\text{rot}}(J_{K_A K_C}) \cdot \Phi_{\text{bend}}(\nu_2; \gamma) \cdot \Phi_{\text{elec}}(A', A'') \} \cdot \Phi_{\text{stretch}}(\nu_1, \nu_3; r, R). \quad (6)$$

The first part $\{ \dots \}$ of Eq. (6) is the electronic and angular, and the second the radial. As will be shown later only the first part enters into the Franck–Condon formula.

In the first absorption band of water the electronic transition is between the A' and A'' state. This transition is perpendicular with the dipole moment μ perpendicular to the H₂O plane. With space fixed polarization vector ϵ , $\mu \cdot \epsilon$ is a function of the H₂O orientation angles in space too. We denote the angular part: $\mu \cdot \epsilon_{\text{ang}}$.

The dissociation process can be divided into two steps. The first treats the photon absorption:

$$\langle A' | \epsilon \cdot \mu | A'' \rangle \approx \epsilon \cdot \mu_{\text{ang}}, \quad (7)$$

where an electron is transferred from the A' to the A'' orbital,³¹ and the nuclear coordinates are held fixed. In the second step H₂O fragments along the A'' surface. In general this surface couples the electronic and rotational degrees of freedom during the fragmentation and angular and the electronic part of the scattering wave function is coupled with the radial motion. In the general case, Eq. (3) cannot be reduced to an integral over angles and electronic coordinates only.

Only if the final state interaction is negligible does the scattering wave function decouple. In the case of water in the first absorption band the final state interaction is small for the rotational and electronic degrees of freedom, and the angular and electronic part of the scattering wave function

can be separated from the dissociation coordinate and Eq. (3) can be simplified.

Here the electronic and angular scattering wave function does not depend on the radial H–OH coordinate which holds up to the asymptotic limit of a free OH rotor described by the OH quantum states $p = \mp 1$, $\Omega = 1/2, 3/2$, and j . The Franck–Condon formula is a simple integral over electronic and angular coordinates of the H₂O wave function and the coordinate representation of the free rotor base, taking the dependence of $\epsilon \cdot \mu$ on the orientation of the H₂O plane into account.

The coordinate representation of the free rotor function can be obtained by angular momentum coupling. The OH angular momentum j couples with the spin s of the H(²S) atom and the orbital angular momentum l to total J_r . These functions are labeled by the angular momentum quantum numbers $j, \Omega, p, s, m_s, l, m_l$. It should be noted that in difference to the H₂O functions the free rotor functions depend on both electronic and angular coordinates and that they cannot be decoupled due to the fine structure.

With this rotor base the Franck–Condon formula follows:

$$P(J_{iK_A K_C} \rightarrow \Omega, j, p) = \sum_{J_r, s, m_p, l, m_l} |a_{J_r, \Omega, p, s, m_s, l, m_l}| \cdot \langle \Phi_{\text{rot}}(J_{KK}) \cdot \Phi_{\text{elec}}(A'') \cdot \Phi_{\text{bend}}(v_2, \gamma) | \epsilon \cdot \mu_{\text{ang}} | j, \Omega, p \rangle | s, m_s \rangle | l, m_l \rangle |^2 \quad (8)$$

with $a_{J_r, \Omega, p, s, m_s, l, m_l}$ as vector coupling coefficients.

Balint Kurti developed a valence bond model and connected the A'' state with the electronic orbitals of the OH + H system.²² After integration over the electronic degree of freedom and analytic angular integration he reduced Eq. (8) to formula (75) in Ref. 22. Because of the electronic model used, this formula can only be applied for H₂O or the isoelectronic H₂S in the first absorption band, where the fragments OH, SH are in the ² π state. For a different system the model has to be changed.

In comparison to the exact equation (3) the FC formula is an integral over electronic and angular coordinates only. The radial coordinates do not affect the rotational and fine structure populations. Neither the scattering wave function has to be calculated, nor the overlap integral over the radial coordinates has to be done, and the numerical simplification is tremendous. Besides the computational ease we want to stress once more the principal simplification. The FC formula neglects the final state interaction, and the FC probabilities do only tell how much of the free rotor motion is already contained in the parent motion. Forces during the fragmentation which excite rotational and fine structure states are omitted.

The only function that has to be calculated numerically is the angular eigenfunction of the H₂O bound state.¹⁹ This is done numerically using a PES by Sorbie and Murrell.³² Neither the photon energy nor the repulsive PES enters into the Franck–Condon rotational and fine structure distributions.

All the preceding FC formulas^{20,21} did not include the

electronic degrees of freedom and could only be applied for fragmentation into ¹ Σ molecules where no fine structure states exist. They are essentially a projection of the angular part of the bound state on a free rotor base defined by the nuclear angular momentum of the diatomic (¹ Σ) and the orbital angular momentum of the relative motion. The electronic coordinates are completely neglected. For a quantitative description of the photodissociation of H₂O, where the OH fragments shows pronounced fine structure effects, these old FC formulas are not suited.

V. TEST OF THE FC THEORY

A. Comparison with state to state data

In this section we compare the experimental state to state data with the FC data, and prove the validity of the model. Figures 11 to 14 show comparisons of experimental and theoretical OH product state distributions for different initial H₂O states.

The rotational distribution of OH for a series of H₂O rotational states with $J = 4$ are compared in Fig. 11. The initial H₂O quantum state is given in the figure. The data are for the $\Pi^+ \Lambda$ doublet in ² $\Pi_{3/2}$. The open circles represent experimental data and the full circles the theoretical results from the FC theory. The positions at which the experimental data were normalized to theory are indicated by arrows.

The agreement of experiment and theory is obviously very nice. The FC theory predicts all maxima and minima exactly where they are found experimentally. The small deviations may be either due to experimental error, or to some remaining small final state interaction. However, the present signal/noise ratio does not allow to discriminate between these alternatives.

In some cases electronic fine structure distributions have also been measured. The comparison of these distributions is given in Fig. 12 for the H₂O rotational states 4_{04} and 4_{14} . The normalization is the same as in Fig. 11.

Again the agreement is very good, especially because no separate normalization is used. This implies that the theory describes *relative* populations in the fine structure components correctly. This is important because the relative population of Λ doublet states is one of the most interesting aspects in the photodissociation of H₂O. Unfortunately no experimental data are available for ² $\Pi_{3/2}^+$, $j = 3.5$.

Figure 13 shows a comparison of experiment and theory for the photodissociation of the 0_{00} rotational ground state of H₂O. Shown are the distributions for the ² $\Pi_{3/2}$, [Fig. 13(a)] and the ² $\Pi_{1/2}$ [Fig. 13(b)] multiplet states. Open symbols are for the experiment and filled symbols for theory. Circles are for the $\Pi^+ \Lambda$ doublets (probed by R lines) and squares for the $\Pi^- \Lambda$ doublet (probed by Q lines). In this case the theoretical curves are normalized to the experiment using the area below the ² $\Pi_{3/2}^-$ rotational distribution.

Qualitatively the distributions are all very nicely reproduced by the FC theory. For example, the fast decay for the $\Pi^+ \Lambda$ doublet in ² $\Pi_{3/2}$, the increase in the $\Pi^- \Lambda$ doublet in ² $\Pi_{3/2}$ going from $j = 1.5$ to 2.5 as well as the decrease later on, and the shoulder at $j = 5.5$ are reproduced in the theory. The relative population in the Λ doublet states, especially the anti-inversion at $j = 1.5$ and the inversion later on is also

predicted in the theory. The largest deviations are found for larger j , where the structure is more pronounced in theory than in experiment.

For the $^2\Pi_{1/2}$ multiplet state only the population in the

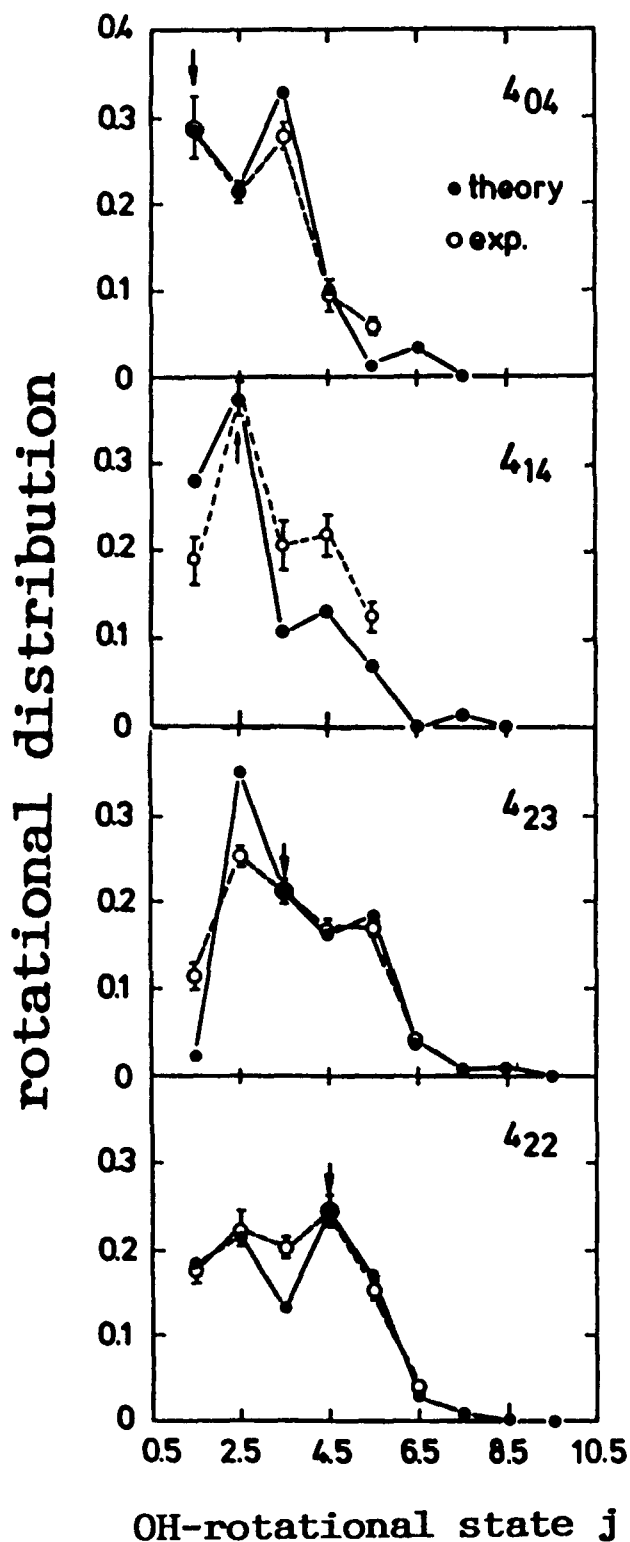


FIG. 11. Comparison of experimental (open circles) and theoretical (full circles) OH product state distributions for several quantum states of H₂O with $J=4$. The H₂O rotational quantum numbers are given in the figure. The data are for the $\Pi^+ \Lambda$ doublets in $^2\Pi_{3/2}$ only. Arrows mark the OH quantum number where theory is normalized to the experiment.

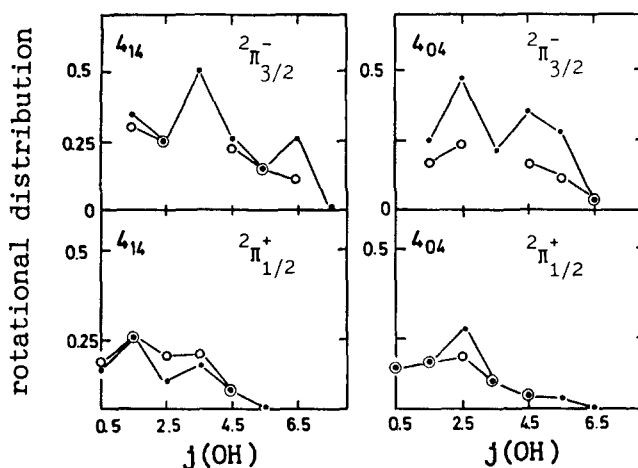


FIG. 12. Comparison of experimental (open circles) and theoretical (full points) OH product state distributions for different electronic fine structure components. Only data are shown for the 4_{14} and 4_{04} H₂O state. The normalization is the same as in Fig. 11.

$\Pi^+ \Lambda$ doublet has been measured, but again there is good agreement between experiment and theory.

In this section we compared the experimental state to state data with the Franck-Condon probabilities. As the theory so nicely matches the experiment, we have proved that the final state interaction for the dissociation of H₂O in the first absorption band is small.

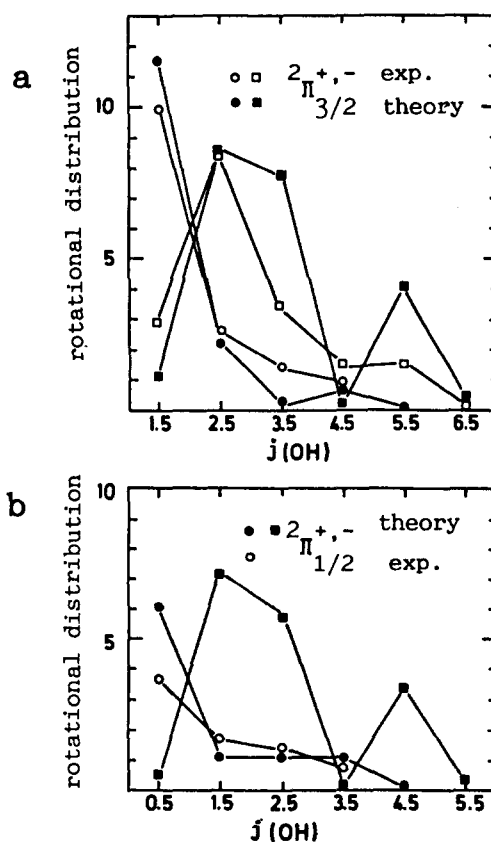


FIG. 13. Comparison of experimental (open symbols) and theoretical (close symbols) OH state distributions for the 0_{00} state of H₂O. (a) shows the results for $^2\Pi_{3/2}$. The squares denote the $\Pi^- \Lambda$ doublet and the circles the $\Pi^+ \Lambda$ doublet. (b) shows the corresponding data for $^2\Pi_{1/2}$, where the same symbols have been used. Unfortunately, no experimental data are available for the $\Pi^- \Lambda$ doublet in $^2\Pi_{1/2}$.

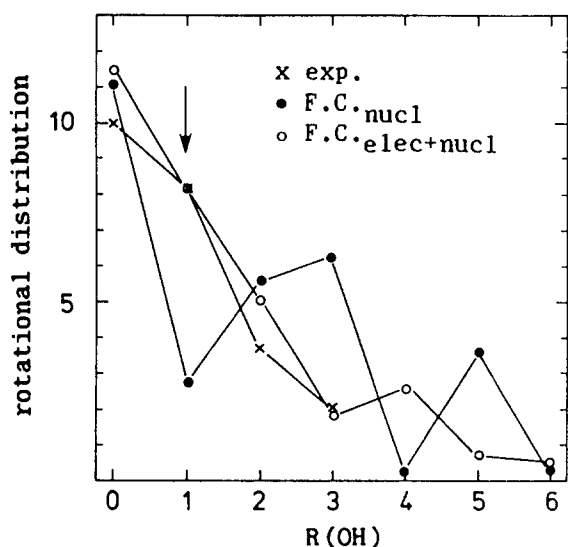


FIG. 14. Comparison of the old Franck–Condon theory which does not treat the electrons and only projects the nuclear motion (FC_{nuc1}) and the theory used here ($FC_{\text{elec} + \text{nuc1}}$), which includes the fine structure, with the experiment. H₂O was dissociated out of its ground state 0_{00} . The experiment is averaged over the Λ doublets and $FC_{\text{elec} + \text{nuc1}}$ is summed over all fine structure states. The OH rotational quantum number is given by the pure nuclear rotation $R = N - 1$.

If a dissociation process can be described in the Franck–Condon limit, the product distributions depends sensitively on the parent quantum state. To any dissociation experiment with insufficient initial state preparation (like bulk or nozzle experiments) many parent states contribute, and the product state distributions are averaged over initial quantum states. As the final state interaction might smear out the product state distribution too, one cannot distinguish between the two effects: final state interaction on the one side

and averaging over initial quantum states on the other side. Only from state to state data shown here can a good estimate of the final state interaction be gained.

This FC formula is the first that includes electronic degrees of freedom. Only then a quantitative comparison with the fine structure and rotational distributions of the fragment OH(²Π) is possible. In Fig. 14 we compare the old Franck–Condon theory which is only a projection of the nuclear parts of the wave functions^{20,21} (FC_{nuc1}) with the experiment and the theory we use, which also contains the electronic degrees of freedom ($FC_{\text{elec} + \text{nuc1}}$). As the fine structure is omitted in FC_{nuc1} we averaged $FC_{\text{elec} + \text{nuc1}}$ over the Λ doublet and spin doublet niveaus. The experiment is only summed over the Λ doublet states, because the $^2\Pi_{1/2}^-$ fine structure niveau has not been measured. As can be seen in the figure, $FC_{\text{elec} + \text{nuc1}}$ describes the experiment nicely, whereas FC_{nuc1} is strongly structured and does not reproduce the experimental data. Only after averaging over the structure, is the comparison fair.

B. Simulation of the photodissociation of H₂O at different temperatures—comparison with bulk and nozzle experiments

In all the state to state data the general structure in the distributions is surprisingly very well reproduced in the theory. This good agreement gives considerable faith in the application of the FC theory. With this FC formula we have the tool to calculate the OH state distribution for any initial H₂O rotational state, and to model the H₂O photodissociation at different parent temperatures.

In Fig. 15 we plot the rotational distributions of the two Λ doublet states in $\Omega = 3/2$ for $J(\text{H}_2\text{O}) = 0$ to 3. The circles and squares denote the Π^+ and Π^- Λ doublet, respectively.

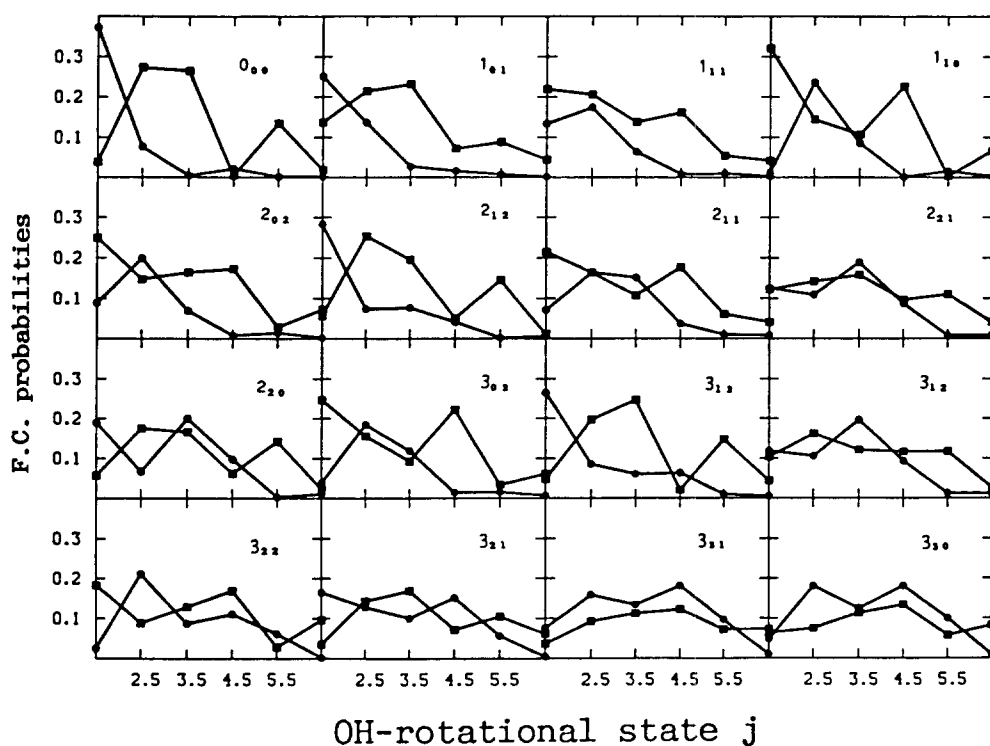


FIG. 15. Oh product state distributions predicted by the FC theory for H₂O rotational states with $J = 0$ to $J = 3$ and all corresponding projection quantum numbers. The points mark the Π^+ Λ doublet and the squares the Π^- Λ doublet in $^2\Pi_{3/2}$.

The distributions look similar to those already discussed. They are strongly structured, showing maxima and minima with the Λ doublets out of phase. The distributions get broader with increasing rotational quantum number, indicating that the initial rotational angular momentum is transferred to the fragment.

Now we have the possibility to synthesize the product state distributions at different H₂O temperatures. This is particularly interesting, because the experimentally found inversion among the Λ doublets is responsible for OH maser action in the interstellar space,¹⁶ and a prediction of the temperature dependence of the inversion is important for astrophysical applications. We can especially compare these results with the experiments done using a supersonic nozzle expansion to cool the rotational degree of freedom of water⁹ and with the bulk experiments done at 157⁹ and 193 nm.

At a given temperature the H₂O molecules will be distributed over different rotational states according to the Boltzmann statistics. The probability of forming OH in a quantum state Ω, j, p when water of the temperature T is photolyzed is simply obtained by weighting the state to state product distributions for all initial H₂O rotational state by their Boltzmann factor and adding them together. With σ_{if} as the state to state probability, and $p_i(T)$ as the Boltzmann weight the procedure is simply

$$\sum_i p_i(T) \cdot \sigma_{if}. \quad (9)$$

The results are given in Table III for the two Λ doublet states in the $\Omega = 3/2$ spin manifold. For the present data the calculations were extended up to $J(\text{H}_2\text{O}) = 6$. Therefore the Boltzmann average is converged only for temperatures below 150 K. The contribution of higher rotational states, which are neglected here, will tend to increase the OH rotational temperature, especially for higher H₂O temperatures.

The OH temperatures are calculated by a least square fit of the FC data with a Boltzmann curve. The standard deviation, which is also given in the table indicates the deviation from a true Boltzmann distribution. Our data show that the

TABLE III. Dependence of the fragmentation process on the H₂O temperature. The OH rotational distributions for the ${}^2\Pi_{3/2}^-$ are fit by a Boltzmann curve and the resulting temperatures and the standard deviation of the temperature is listed vs the parent temperature.

H ₂ O temperature (K)	Temperature of the OH fragment (K)	
	${}^2\Pi_{3/2}^-$	${}^2\Pi_{3/2}^+$
10	413 ± 101	168 ± 25
20	389 ± 46	172 ± 24
30	383 ± 25	176 ± 21
40	387 ± 16	180 ± 17
50	393 ± 10	185 ± 13
60	401 ± 7	192 ± 10
80	420 ± 3	209 ± 5
100	438 ± 2	229 ± 3
150	482 ± 2	280 ± 3
200	522 ± 3	328 ± 4
250	556 ± 4	370 ± 5
300	585 ± 5	408 ± 6

OH distributions are close to Boltzmann even at low temperatures $T \geq 30$ K. This is remarkable: Although the state to state distributions are strongly structured this structure gets smeared out if more initial states contribute to the fragmentation.

As can be seen from Table III, the OH temperature rises with the H₂O temperature. This is not surprising since the FC model projects bound states on a free rotor base and the initial angular momentum is transferred to the fragments. This can also be seen from Fig. 10 where the rotational excitation is larger for $J(\text{H}_2\text{O}) = 4$ than 0. Also has to be mentioned, that the rotational temperature of the $\Pi^- \Lambda$ doublet is always above the temperature of the $\Pi^+ \Lambda$ doublet which points to a Λ doublet effect which will be discussed later.

The comparison with the experiment where water was expanded through a nozzle and its rotational temperature was lowered, is almost quantitative. In this experiment with cold H₂O a rotational temperatures of 475 K for the Π^- and 210 K for the $\Pi^+ \Lambda$ doublet, respectively, was found. This matches our data, assuming an experimental error of about 10%. The actual H₂O temperature in the nozzle expansion is not measured yet. From our data we conclude a temperature in the range 20–100 K where an agreement with the experiment is good.

We have only proved that the dissociation of H₂O excited in the asymmetric stretch vibration can be treated in the Franck–Condon limit. As has been pointed out already, the vibrational and photolysis energy add up to 180 nm. As the final state interaction is negligible, the repulsive PES probed during the fragmentation does not exert any torque on the OH molecule at this energy. At 157 nm however different parts of the repulsive potential surface are accessed. At this wavelength the final state interaction is possibly larger, and rotational states are coupled to the dissociation coordinate.

The effect of the final state interaction can roughly be estimated to be small, as the differences between the Franck–Condon calculations and the nozzle experiment are small too. However, for a quantitative analysis a state to state experiment has to be done at higher dissociation energies.

Bulk experiments have been done at two dissociation wavelengths, 157 and 193 nm. At 157 nm both Λ doublet states were found to be equally populated with a rotational temperature of 930 K.⁹ At 193 nm a small Λ doublet effect is still found and the measured rotational temperatures are 457 and 379 K for the upper and lower Λ doublet state, respectively. This result shows the limit of the FC theory. The FC formula is independent on the wavelength and cannot explain different results at different dissociation wavelength. The FC rotational temperature is with 585 and 408 K, respectively, in between the two experiments.

This difference might be due to the possible final state interaction for the experiment at 157 nm, which results in warmer fragment distributions. Besides that, there is a principal limit for the application of the FC theory to model high parent temperatures. By simple averaging over the initial H₂O states according to a Boltzmann statistic one completely neglects the dependence of the absorption cross section on the rotational state. This dependence might be complicated and explain differences for 157 and 193 nm photolysis. This

dependence is not included in our model for higher H₂O temperatures discrepancies can be expected.

Anyhow the differences are not that drastic, when plotting the rotational distributions in a linear scale, as can be seen in Fig. 16. Because of the large OH-rotational constant $B_e = 18.9 \text{ cm}^{-1}$ small differences in linear plot result in relatively big deviations in the corresponding temperature. Shown are the rotational distributions of OH in a linear scale for the bulk experiment at 193 and 157 nm and the FC calculations for $T = 300 \text{ K}$. In the linear plot the maximum is only shifted by one quantum number when comparing the different curves, and the distribution for 157 nm is broadened by about two quantum numbers. Clearly, these differences are detectable in the experiments. But the general result: only a little rotational excitation of the OH fragment compared to the excess energy, can be seen from all of the curves.

As has been mentioned before, the two Λ doublet states are not equally populated in the nozzle experiment at 157 nm and in the bulk experiment at 193 nm. In the following we investigate this Λ doublet effect and its temperature dependence.

First of all we synthesize the experiment at 157 nm where water was cooled in a nozzle expansion and an inversion in the Λ doublets was found. This inversion depends on the OH rotational state j and is more pronounced for higher j 's. The experimental data are shown in Fig. 17 and are denoted by full squares. As the H₂O temperature in the nozzle expansion is not known, we did model calculations for temperatures between 10 and 100 K. For low temperatures, where only a few H₂O states are populated, the inversion is a structured function in j . This is not surprising since for the state to state data the Λ doublets are out of phase and inversion and anti-inversion occur. The more H₂O states contrib-

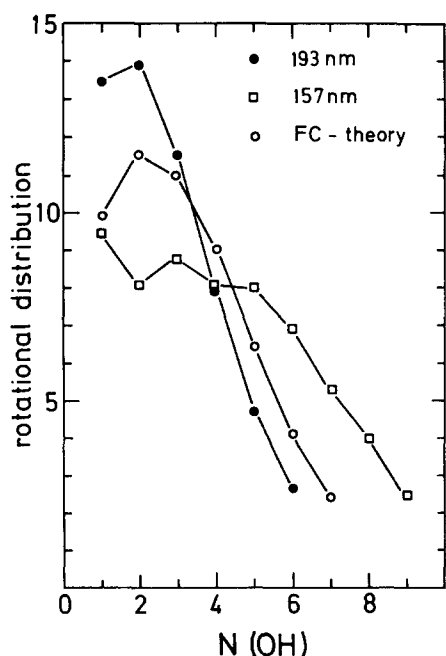


FIG. 16. Linear plot of OH rotational distributions for the bulk experiments done at 193 and 157 nm and the FC calculation for $T(\text{H}_2\text{O}) = 300 \text{ K}$. The curves are normalized to each other by the area from $N = 1$ to $N = 6$.

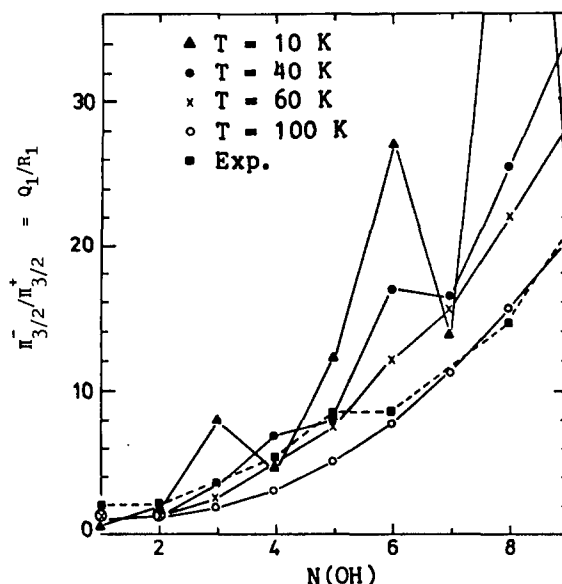


FIG. 17. Λ doublet ratio Π^-/Π^+ for the $\Omega = 3/2$ spin state as a function of $N(\text{OH})$. The broken curve shows the experimental result obtained in the nozzle experiment. The other symbols denote Franck-Condon calculations for different initial H₂O temperatures. The temperatures are given in the figure.

ute, i.e., at higher temperatures, these structures get completely smeared out, and the Λ doublet ratio is a smooth function in j . For initial temperatures $T(\text{H}_2\text{O}) \geq 10 \text{ K}$ a strong preference of the upper Λ doublet state is found, which similar to the experiment increases with j . Comparing the experimental and theoretical curves shows again a good agreement though one cannot conclude an experimental H₂O temperature. All theoretical curves for $T(\text{H}_2\text{O}) = 20$ –100 K fit the experimental data about as good. Again final state interaction for the experiment at 157 nm might explain the differences.

The bulk experiment has been done at two dissociation wavelengths, 157 and 193 nm. At 193 nm an inversion in the Λ doublets was found too. As in the nozzle experiment it is a monotonic function of j , but the inversion is less. The model calculations show the same tendency: An inversion increasing with j but less strong compared to the Λ doublet ratio at lower temperatures. At 60 K H₂O temperature the inversion ratio at $N(\text{OH}) = 7$ is about four times larger than at 300 K.

The bulk data at 157 nm are taken at fairly high pressures and large delays, so that the Λ doublets which are known to quench very efficiently might already be relaxed.²⁹

As can be seen in Fig. 18, which shows the Λ doublet ratio for the dissociation of room temperature H₂O, the theoretical Λ doublet ratio is always larger than the experimental one. But the tendency, less inversion with higher H₂O rotational temperature, is clearly reproduced by the FC model. The discrepancy between experiment and theory might even get smaller if more H₂O rotational states were averaged. As has been mentioned before, with $J(\text{H}_2\text{O}) = 0$ –6 the Boltzmann average only converges for temperatures smaller than 150 K. The higher H₂O states $J > 6$ will make the Λ doublet effect smaller.

The nozzle and bulk data compared to the state to state

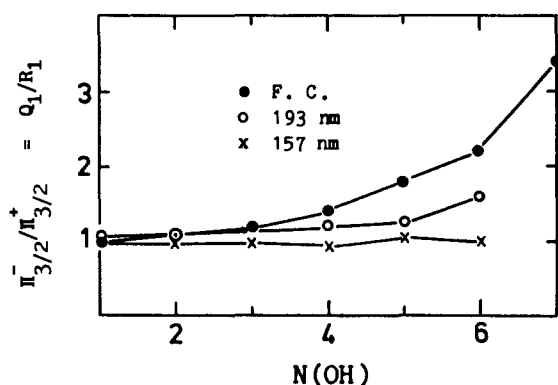


FIG. 18. A doublet ratio Π^-/Π^+ for the $\Omega = 3/2$ spin state at room temperature. ●: Franck–Condon theory for 300 K. ○: Experiment done at 193 nm. ×: Experiment done at 157 nm.

experiment demonstrates once more that a complete preparation of the initial H₂O state is necessary for the understanding of the dissociation process. The structures in rotational and fine structure distribution which are characteristic for the dissociation of H₂O can only be seen in state to state experiments. Even at low H₂O temperatures as achieved in the nozzle expansion, too many H₂O states contribute, and the structures are averaged out.

As a resume the FC model turned out to reproduce the preceding experiments under bulk and nozzle conditions at least qualitatively. This holds for rotational and fine structure distributions.

VI. DISCUSSION

A. Investigation of the repulsive potential surface—validity of the FC approximation

As has been mentioned before, the main assumption of this Franck–Condon approximation is that the final state interaction for the rotational and electronic degrees of freedom is small.

The mechanisms for rotational excitation are well understood from scattering theory. The anisotropy of the potential surface $dV/d\gamma$ is the torque acting on the diatomic and thus the reason for rotational excitation. γ is the angle between the OH vector and the distance vector between the H atom and the center of mass OH.

As the FC theory reproduces the experimental data, no rotational excitation is observed, and only parts of the repulsive PES with small or no anisotropy are probed.¹⁹ This can be seen when looking at the *ab initio* PES in Fig. 19. At fixed OH distance the dependence of the A'' PES on the orientation angle is plotted for fixed OH–H radial distances. Also shown is the angular dependence of the H₂O bound wave function, which is a Gaussian function peaking at 104°. This Gauss function represents the angular coordinates, which are prepared on the A'' PES after the photon absorption.

Though the A'' surface has areas with strong anisotropy, the anisotropy is negligible for the coordinate window prepared by the geometry and zero point motion of the bound state. As this holds for all radial OH–H distances energetically allowed, it is obvious that only parts of the PES with small anisotropy are probed. By looking at the A'' surface

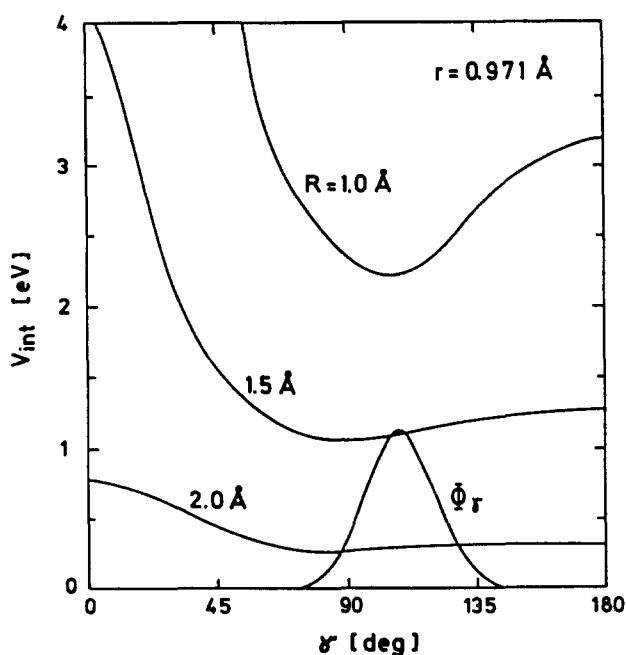


FIG. 19. Angular variation of the A'' potential surface for different H–OH distances R . The OH separation is fixed at its equilibrium value. Φ_r is the angular part of the bond nuclear wave function.

and knowledge of the bound state geometry one can explain why the rotational coupling is negligible and the FC theory works so nicely.

B. Dependence of the FC distributions on molecular parameters

The general assumption of this paper is that the final state interaction for this model system is negligible and the FC model can be applied. In this theory a bound eigenfunction of H₂O is projected on the OH–H free rotor base. Here we want to study the dependence of the fragmentation on molecular parameters like bond angle and spin–orbit constant of the fragment.

For $J(\text{H}_2\text{O}) = 0$ the H₂O wave function is extremely simple. It is a Gaussian like function peaking at about 104°. In order to study the dependence of the fragmentation on the bond angle, we simply modified the Gauss function and varied the maximum position, and did FC calculations. The FWHM has been kept fixed.

The results are shown in Fig. 20 where the bond angles are varied between 170° and 90°. The bond angle effects the distribution markedly. For almost linear molecules $\gamma = 170^\circ$ the distributions are smooth with almost no structure and the lower Λ doublet state is more populated. The situation changes considerably if the molecule becomes increasingly bent. At 150° the distributions becomes structured already and at high j a preference for the upper Λ doublet state is found. The angle 110° is close to the true bond angle in H₂O and the distribution looks similar to the one discussed earlier in Fig. 13.

At 90° the oscillatory structure is most interesting. The population in the two Λ doublet states is oscillating with a period of one going to zero in between. The oscillations are

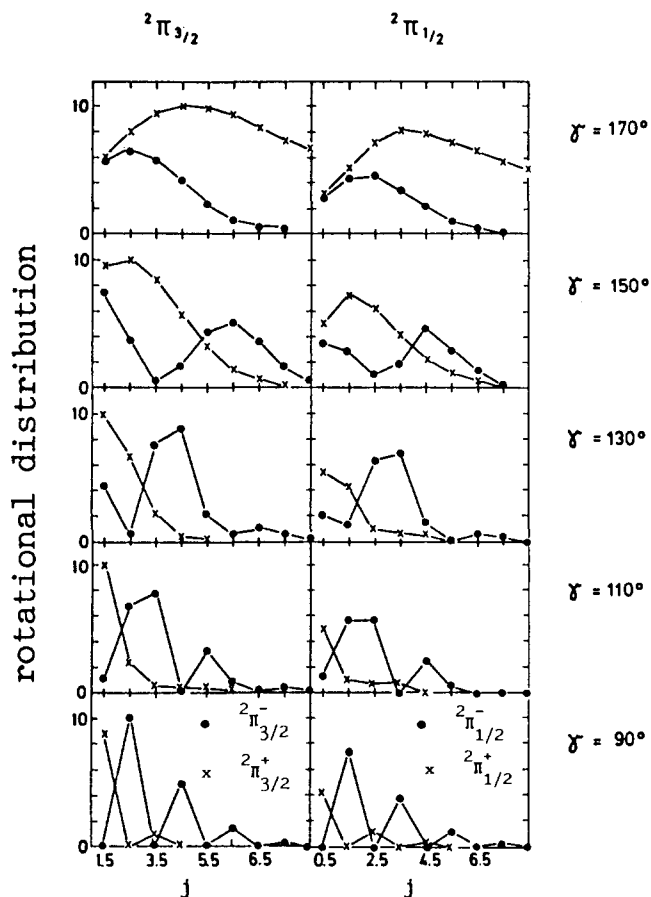


FIG. 20. Model Franck-Condon calculations for the dependence of the state distribution on the H₂O bond angle γ . The bond state wave function is a Gauss function peaking at different angles which are denoted in the figure. The FWHM is 20° for all calculations. Shown are rotational distributions for all fine structure states which are labeled in the figure.

opposite for the two Λ doublet states and opposite for the same Λ doublet states and same j in the two multiplet states.

It should be noted, that these calculations except the calculations for 90° represent an artificial molecule. If H₂O had a different bond angle and the dissociation were Franck-Condon the results are those given in Fig. 20. The isoelectronic molecule H₂S has a bond angle of about 90°, and the model calculations for that angle were the Franck-Condon distributions for H₂S neglecting the difference in λ . As no state to state data are available yet, a comparison of experiment and theory on a state to state level cannot be done.

The bond angle is the most important degree of freedom of the bound state. Now we want to study the dependence of the FC distributions on the degrees of freedom of the free rotor base. This base is determined by angular momentum algebra and depends for example on how the electrons of OH couple to the nuclear motion. In all the preceding calculations we treated the OH molecule in the intermediate coupling case³³ where OH changes from Hund's case (a) for small j to Hund's case (b) for large j 's. By artificially changing the ratio of spin-orbit constant to rotational constant $\lambda = A/B_{\text{rot}}$ one can create a molecule coupled according to Hund's case (a) ($\lambda = 1000$) or Hund's case (b) ($\lambda = 0$) coupling scheme.

The results are shown in Fig. 21 for the dissociation of

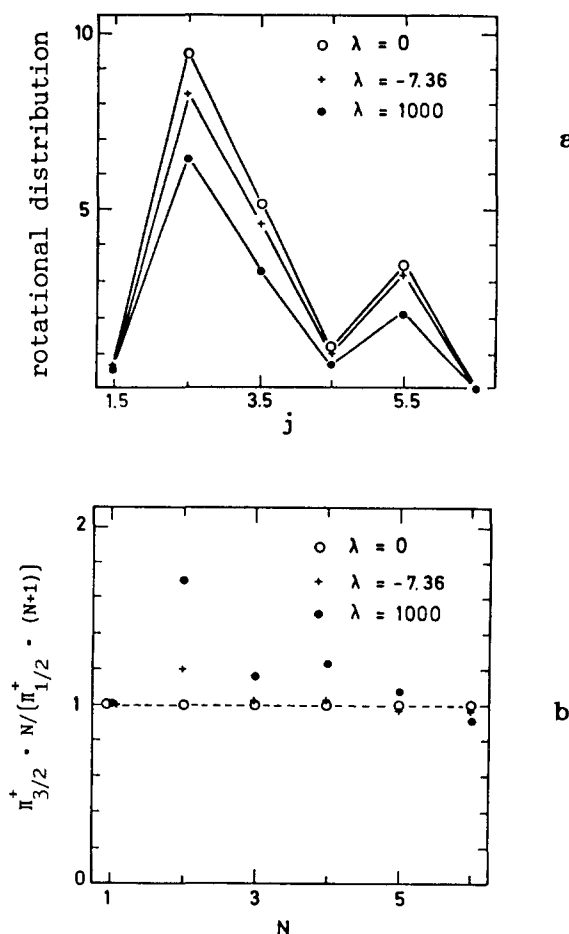


FIG. 21. Effect of Hund's coupling cases on the product state distribution for the photodissociation of the 0_{00} state of H₂O. $\lambda = 0$ corresponds to Hund's case (b), $\lambda = -7.36$ to the case of OH, and $\lambda = 1000$ to Hund's case (a). (a) shows rotational distributions for the $\Omega = 3/2$, $p = +1$ fine structure state $2\Pi_{3/2}^+$ and (b) the relative spin distribution.

the H₂O ground state $J_{K_A K_C} = 0_{00}$. The rotational distribution hardly changes as can be seen from Fig. 21(a). For all values of λ the corresponding curves are almost on top of each other.

As can be expected when changing the spin-orbit constant which favors energetically one spin state over the other, the relative spin population is more affected. Figure 21(b) shows the ratio of the two spin states divided by their degeneracy, which implies that a value of one corresponds to a statistical distribution. For Hund's case (b) ($\lambda = 0$) which means no spin-orbit coupling, we obtain a strictly statistical distribution for the spin states. For the case of OH, which is obtained for $\lambda = -7.36$, the distributions are almost statistical with a small preference of the $\Omega = 3/2$ spin state at $N = 2$. For Hund's case (a) molecules ($\lambda = 1000$) there is a stronger effect, again in favor of $\Omega = 3/2$.

These model calculations show how the photon absorption, which means the perpendicular Franck-Condon projection alone, can cause nonstatistical populations for Λ doublet and spin states. Even for systems with strong rotational coupling during the fragmentation the ratio of the fine structure states might still be given by the FC transition. New experiments will hopefully give deeper insight in the

importance of the perpendicular Franck–Condon transition for fine structure distributions.

The theory as it has been derived by Balint-Kurti²² can only be applied for H₂O fragmenting into OH(²Π) or the isoelectronic system H₂S. Even for similar molecules like NO₂, where the diatomic is still in the ²Π state the model has to be modified, because the electronic structure is different. The atom for example can be formed in the different spin states O(³P)³⁴ or O(¹D).³⁵ To understand the nonstatistical population of electronic fine structure states for other systems too, the FC model has to be extended.

There have been a lot of experiment done in recent years, where a selective population of electronic fine structure states has been measured. This is true for Λ doublet states³⁶ and for spin states.^{10,37} One interesting question is whether this selectivity is due to the Franck–Condon step or due to final state interaction during the fragmentation. As has been shown here, the selectivity can be expected from the simple Franck–Condon projection.

VII. CONCLUSION

We dissociated single rotational states of vibrationally excited H₂O and detected the OH fragment state selectively with LIF. The method of using IR radiation to prepare a quantum state and also to enhance the absorption cross section is new and can also be applied for a variety of systems. It allowed us to characterize the parent molecule completely in rotational and vibrational quantum numbers.

The H₂O state was prepared with a tunable IR laser operating at around 2.7 μm in single rotational states of the asymmetric stretch vibration. At the dissociation wavelength of 193 nm the absorption cross section of this one state is enhanced and its fragmentation can be detected.

We measured the OH state distribution after photolysis of different H₂O rotational states. The OH distribution depends sensitively on the parent state. This holds for rotational and Λ doublet distributions. The spin states are within experimental resolution statistically populated.

The rotational distributions for each fine structure niveau are strongly structured, showing maxima and minima. Different Λ doublet components are out of phase. When one state is most populated the other one is least populated. The Λ doublet ratio is a structured function of *j*(OH) too and varies between inversion and anti-inversion.

In proceeding dissociation experiments in the first dissociation band of H₂O with incomplete state preparation the OH distributions were not structured but smooth functions in *j*(OH). This points to the necessity of complete characterization of the parent state in order to detect the main features of the dissociation process.

A simple Franck–Condon theory which includes the rotational and electronic degree of freedom reproduces the experimental state to state data excellently. This holds for rotational and fine structure distributions. The validity of the Franck–Condon approximation can also be seen when analyzing the anisotropy of the *A*'' potential energy surface.

With this Franck–Condon formula the dissociation of any H₂O quantum state can be calculated, and by proper

averaging, initial H₂O temperatures can be synthesized. We found at least qualitative agreement of the FC data with all the preceding experiments, where water was photolyzed under bulk and nozzle conditions.

Even the experiment with jet cooled water does not show any structure. As modeled by the FC calculations these structures cancel if too many H₂O states contribute to the signal. Once more the necessity of complete initial state preparation is obvious.

Within the FC approximation we performed model calculations. We studied the dependence of the fragmentation on the H₂O bond angle and on the spin–orbit constant of OH. This helps for different systems to predict the FC distribution and by comparing with the experimental data to study the influence of the final state interaction.

¹A. Hodgson, J. P. Simons, M. N. R. Ashfold, J. M. Bayley, and R. N. Dixon, *Chem. Phys. Lett.* **107**, 1 (1984); M. P. Docker, A. Hodgson, and J. P. Simons, *Mol. Phys.* **57**, 129 (1986).

²H. Joswig, P. Andresen, and R. Schinke, *J. Chem. Phys.* **85**, 1904 (1986).

³R. A. Copeland and D. R. Crosley, *J. Chem. Phys.* **81**, 6400 (1984).

⁴D. A. King, R. Haines, N. R. Isenor, and B. J. Orr, *Opt. Lett.* **8**, 629 (1983); W. Meier, G. Ahlers, and H. Zacharias, *J. Chem. Phys.* **85**, 2599 (1986).

⁵D. E. Reisner, P. H. Vaccaro, C. Kittrel, R. W. Field, J. L. Kinsey, and H. L. Dai, *J. Chem. Phys.* **77**, 573 (1982).

⁶P. J. Dagdigian and R. N. Zare, *Science* **185**, 793 (1974); J. L. Kinsey, *Annu. Rev. Phys. Chem.* **28**, 349 (1977).

⁷M. N. R. Ashfold, R. N. Dixon, and R. J. Stickland, *Chem. Phys.* **88**, 463 (1984); J. H. Glowina, S. J. Riley, S. D. Colson, J. C. Miller, and N. N. Compton, *J. Chem. Phys.* **77**, 68 (1982).

⁸H. Okabe, *Photochemistry of Small Molecules* (Wiley, New York, 1987).

⁹P. Andresen, G. S. Ondrey, B. Titze, and E. W. Rothe, *J. Chem. Phys.* **80**, 2548 (1984).

¹⁰I. Nadler, H. Reisler, and C. Wittig, *Chem. Phys. Lett.* **103**, 451 (1984).

¹¹W. G. Hawkins and P. L. Houston, *J. Chem. Phys.* **76**, 729 (1982).

¹²R. Schinke, V. Engel, P. Andresen, D. Häusler, and G. G. Balint-Kurti, *Phys. Rev. Lett.* **55**, 1180 (1985).

¹³P. Andresen, V. Beushausen, D. Häusler, H. W. Lülf, and E. W. Rothe, *J. Chem. Phys.* **83**, 1492 (1985).

¹⁴G. Herzberg, *Molecular Spectra and Molecular Structure II. Infrared and Raman Spectra of Polyatomic Molecules* (Van Nostrand, Princeton, 1945).

¹⁵K. Watanabe and M. Zelikoff, *J. Opt. Soc. Am.* **43**, 753 (1953).

¹⁶P. Andresen, *Astron. Astrophys.* **154**, 42 (1986); *Comments At. Mol. Phys.* **18**, 1 (1986).

¹⁷V. Staemmler and A. Palma, *Chem. Phys.* **93**, 63 (1985).

¹⁸G. G. Balint-Kurti and M. Shapiro, *Chem. Phys.* **61**, 137 (1981).

¹⁹R. Schinke, V. Engel, and V. Staemmler, *J. Chem. Phys.* **83**, 4522 (1985).

²⁰J. A. Beswick and W. M. Gelbart, *J. Phys. Chem.* **84**, 3184 (1980).

²¹M. D. Morse, Y. B. Band, and K. F. Freed, *J. Chem. Phys.* **78**, 6066 (1983); M. D. Morse and K. F. Freed, *Chem. Phys. Lett.* **74**, 49 (1980).

²²G. G. Balint-Kurti, *J. Chem. Phys.* **84**, 4443 (1986).

²³D. J. Brink, D. Proch, D. Basting, K. Hohla, and P. Lokai, *Laser Optoelektron* **3**, 41 (1982).

²⁴C. Camy-Peyret, J. M. Flaud, G. Guelachvili, and C. Amiot, *Mol. Phys.* **26**, 825 (1973); J. Y. Mandin, C. Camy-Peyret, J. M. Flaud, and G. Guelachvili, *Can. J. Phys.* **60**, 94 (1982).

²⁵A. R. H. Cohle, *Tables of Wave numbers for the Calibration of Infrared Spectrometers* (Pergamon, Oxford, 1977); J. M. Flaud, C. Camy-Peyret, and R. A. Toth, *Water Vapour Line Parameters from Microwave to Medium Infrared* (Pergamon, Oxford, 1981).

²⁶L. B. Kreuzer and C. K. N. Patel, *Science* **173**, 45 (1971).

²⁷V. Engel, *Theoretische Behandlung der Photodissoziation von Wasser in der ersten Absorptionsbande*, Max-Planck-Institut für Strömungsforschung, Bericht 14/1986.

²⁸G. H. Dieke and H. M. Crosswhite, *J. Quant. Spectrosc. Radiat. Transfer* **2**, 97 (1962).

²⁹P. Andresen, V. Beushausen, and H. Lülf, *J. Chem. Phys.* (to be published).

- ³⁰M. Weissbluth, *Atoms and Molecules* (Academic, New York, 1978).
- ³¹G. Herzberg, *Electronic Spectra and Electronic Structure of Polyatomic Molecules* (Van Nostrand, Princeton, 1967).
- ³²K. S. Sorbie and J. N. Murrell, *Mol. Phys.* **29**, 1387 (1975); **31**, 905 (1976).
- ³³M. Bertojo, A. C. Cheung, and C. H. Townes, *Astrophys. J.* **208**, 914 (1976).
- ³⁴U. Robra, Thesis, Universität Bielefeld, 1984; K. H. Welge, NATO ASI Ser. B **105**, 123 (1984).
- ³⁵L. Bigio and E. R. Grant, *J. Phys. Chem.* **89**, 5855 (1985).
- ³⁶R. Mariella, B. Lantsch, V. T. Maxson, and A. C. Luntz, *J. Chem. Phys.* **69**, 5411 (1978); K. Kleinermanns and J. Wolfrum, *ibid.* **80**, 1446 (1984); R. Vasudev, R.N. Zare, and R. N. Dixon, *ibid.* **80**, 4863 (1984).
- ³⁷F. Shokoohi, S. Hay, and C. Wittig, *Chem. Phys. Lett.* **110**, 1 (1984); I. Nadler, D. Mahgerefteh, H. Reisler, and C. Wittig, *J. Chem. Phys.* **82**, 3885 (1985).